STUDY OF NUCLEAR ASTROPHYSICS AT CNS AND RIKEN

NAOHITO IWASA
for the R407n, R336n and CRIB collaborations

Department of Physics, Tohoku University, Sendai, Miyagi 980-8578, Japan

1. Introduction

In explosive stellar environments such as hot bottom burning in massive AGB stars, nova explosions in accreting white dwarfs, X-ray bursts in accreting neutron stars, neutrino-driven winds in core collapse supernovae, heavy elements are generated by the rapid proton capture process (rp process), which consists of a sequence of (p,γ) reactions, (α,p) reactions, and β^+ decays. In the rp process of neutrino-driven winds, (n,p) reactions can also occur in the place of β^+ decays with long half-lives(e.g., ^{56}Ni (6 d), ^{64}Ge (64 s), ^{68}Se (36 s)) [1]. The rp process is a strong candidate for the origin of p nuclides, which are stable neutron-deficient nuclides that cannot be produced by the rapid or slow neutron capture processes (r or s processes). In particular, the large abundances of p nuclides such as ^{92,94}Mo, ^{96,98}Ru cannot be explained apart from the rp process [2]. The rp process starts when a breakout occurs from the hot CNO cycle via the ^{18}Ne$(\alpha,p)^{21}$Na and ^{15}O$(\alpha,\gamma)^{19}$Ne reactions. It produces nuclei up to $A\approx110$ [3]. To determine the reaction path and mechanism of the rp process, it is highly desirable to experimentally measure the (α,p), (p,γ), and (n,p) reaction rates.

This paper describes recent experimental studies of Coulomb dissociation of ^{36}Ca and ^{27}P for investigating the ^{35}K$(p,\gamma)^{36}$Ca and ^{26}Si$(p,\gamma)^{27}$P reactions [4], proton elastic scattering of ^{26}Si for the ^{26}Si$(p,\gamma)^{27}$P reaction [5], and direct measurements of the ^{18}Ne$(\alpha,p)^{21}$Na reaction using a helium active target. The γ width of the first 2^+ resonance state of ^{36}Ca may be larger than the proton

width. Indeed, this state was found by a γ-ray measurement [6]. The role of the ^{35}K(p,γ)^{36}Ca reaction in the rp process is not evident. However in view of the nuclear structure, it is desirable to determine the reduced transition probability $B(E2)$ of ^{36}Ca, because the excitation energy of the 2_1^+ state (0.4 MeV above the proton threshold) is 0.3 MeV lower than that in the mirror nucleus ^{36}S. This large mirror energy difference has been discussed in the framework of shell model calculations using a ^{16}O core, the *sd* shell isospin symmetric interaction and experimental single-particle energies of ^{17}O and ^{17}F [6]. The ^{26}Si(p,γ)^{27}P reaction is pertinent to the production of ^{26}Al, which is the first cosmic radioactivity ever detected through the characteristic 1.809 MeV γ rays of the daughter nucleus ^{26}Mg and concentrated in the galactic plane. While various possible sites are discussed, the origin of ^{26}Al is not yet clear due to large uncertainty regarding its production mechanism. The ^{26}Si(p,γ)^{27}P reaction competes with β^+ decay of ^{26}Si to ^{26m}Al which can produce ^{26}Al via thermal excitation. The ^{26}Si(p,γ)^{27}P reaction is thus important for estimating the production of ^{26}Al. The ^{18}Ne(α,p)^{21}Na reaction is of critical importance for estimating the flow of the rp process because it is the dominant breakout reaction from the hot CNO cycle to the rp process, as mentioned above.

The Coulomb dissociation method is a powerful tool for studying (p,γ) reactions. To deduce the $A(p,\gamma)B$ reaction cross section by this method, the cross section of the dissociation of B into A and proton in the Coulomb field of a high-Z target is measured as a function of the relative kinetic energy. Since this dissociation processes can be regarded as the absorption of a virtual photon, the dissociation cross section can be converted to the $B(\gamma,p)A$ reaction cross section. The $B(\gamma,p)A$ reaction is directly related to the $A(p,\gamma)B$ reaction. This method has the following advantages; (i) the Coulomb dissociation cross section is larger than the proton capture cross section; (ii) it does not require radioactive targets; (iii) thicker targets can be used; (iv) it is expected to have a high detection efficiency due to high-energy charged-particle measurements. We have used the Coulomb dissociation method to study several reactions. They include the ^{7}Be(p,γ)^{8}B [7] and ^{13}N(p,γ)^{14}O [8] reactions and the deduced (p,γ) cross sections are consistent with those obtained by the direct method.

2. Coulomb dissociation of ^{36}Ca and ^{27}P

Experiments were performed using a part of the RI-Beam-Factory (RIBF) accelerator complex operated by RIKEN Nishina Center and Center for Nuclear Study, University of Tokyo. Lead targets with 244- and 125-mg/cm^2 thicknesses were bombarded by ^{36}Ca and ^{27}P beams at 58.0 and 54.2 MeV/u produced by RIPS, respectively. The ^{nat}Pb(^{36}Ca,^{36}Caγ), ^{nat}Pb(^{36}Ca,^{35}K p), ^{nat}Pb(^{36}Ca,^{34}Ar 2p), and ^{nat}Pb(^{27}P,^{26}S p) reactions were studied. The reaction products were measured by silicon detector telescopes and a plastic scintillator hodoscope. The silicon detectors in the first and second layers in the telescope had 5-mm- pitch strip electrodes to measure the position at which the products striked. Since protons penetrated the telescope, their kinetic energies were obtained by measuring the time of flight (TOF) between the target and the hodoscope. An array of NaI(Tl) scintillation counters was placed around the target to measure deexcitation γ rays.

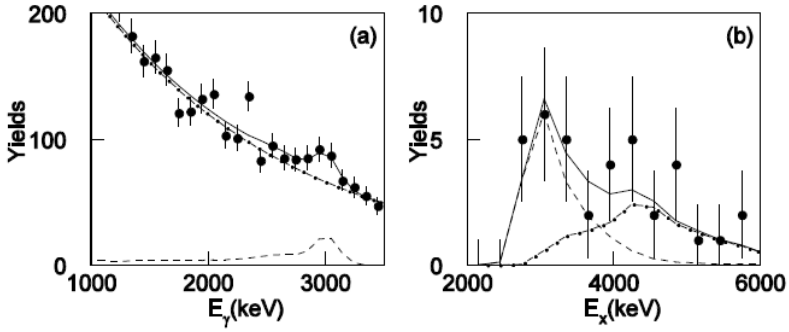

Fig.1. (a) γ energy spectrum for the Pb(^{36}Ca,^{36}Caγ) reaction after correcting the Doppler shift. The solid curve represents the best fit by the simulated line shape for an excited state of 3.0 MeV (dashed curve) and an exponential background (dot-dashed curve). (b) p-^{35}K coincidence yields plotted as a function of the excitation energy of ^{36}Ca. The solid curve represents the best fit by the detector responses for the resonance at 3.0 and 4.3MeV calculated by Monte Carlo simulations.

Figure 1(a) shows the γ energy spectrum after Doppler-shift correction when both the incident particle and the reaction product were identified as ^{36}Ca. A peak is observed at 3.02 (6) MeV, which corresponds to the γ line of the $2_1^+ \rightarrow 0_{gs}^+$ transition; it was reported to be located at 3.015 (16) and 3.036 (11) MeV by Doornenbal *et al*. [6] and Bürger *et al*. [9], respectively. The solid curve represents the best fit by the detector response obtained by a Monte

Carlo simulation using GEANT3 [10] and an exponential background. The *p*-^{35}K coincidence yields are plotted in Fig. 1(b) as a function of the excitation energy of ^{36}Ca calculated from the angles and momenta of ^{35}K and protons. The spectrum can be fit with two peaks: one corresponds to the 3.0 MeV γ peak, while the other one is located at about 4 MeV. The fits give a peak energy of 4.3 MeV for the higher-energy peak. The peak at 4.3 MeV can be tentatively assigned to be the second 2^+ state because the excitation energy of the mirror state in ^{36}S is at 4.575 MeV, which is close to 4.3 MeV. The large *E*2 virtual photon flux in the Coulomb excitation supports this assignment. The cross section of the ^{nat}Pb(^{36}Ca,^{36}Caγ) and ^{nat}Pb(^{36}Ca,^{35}K *p*) reactions via the 2_1^+ resonance state were deduced to be 35±6, and 3.3±0.9 mb, respectively. No significant events were observed around 3.0 MeV in the spectrum of 2*p*-^{34}Ar coincidence. An upper limit for the cross section of the ^{nat}Pb(^{36}Ca,^{34}Ar 2*p*) reaction via the 2_1^+ resonance state was estimated to be 2 mb. The cross section to populate the 2_1^+ state in ^{36}Ca was deduced to be 38^{+8}_{-6} mb. The corresponding *B*(*E*2; $0^+_{gs} \rightarrow 2^+_1$) value was obtained to be $71^{+17}_{-13} e^2$fm^4 by a distorted-wave calculation using the coupled-channel code ECIS97 [11]. Optical potential parameters determined from elastic scattering data for ^{40}Ar + Pb at 41 MeV/u [12] and the nuclear deformation parameter calculated using the Bernstein prescription [13] were employed. This *B*(*E*2) value is the smallest of all calcium isotopes (including the double-closed nucleus ^{40}Ca) and for *N* = 16 isotones except for ^{22}C and ^{24}O. On the other hand, the present result is larger than that (16 e^2fm^4) predicted by shell model using the USD interaction. This may imply that ^{36}Ca consists of ^{40}Ca + 4n holes with a slightly deformed or polarized ^{40}Ca core. The branching ratio for the decay of the 2_1^+ state was deduced to be $\Gamma_\gamma/\Gamma_p = 10 \pm 3$ from the measured ^{nat}Pb(^{36}Ca,^{36}Caγ) and ^{nat}Pb(^{36}Ca,^{35}K *p*) cross sections.

The reaction rate for the narrow resonance is expressed by

$$N_A\langle\sigma v\rangle = \frac{1.54 \times 10^{11}}{(AT_9)^{3/2}} \omega\gamma \exp\left(-\frac{11.605E_r}{T_9}\right)$$

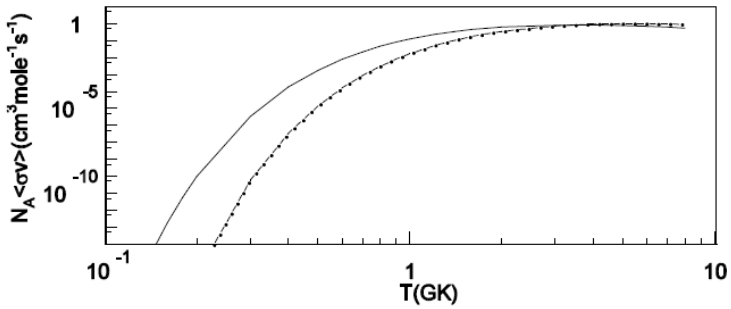

Fig. 2. Temperature dependence of the resonance component of the reaction rate for the ^{35}K(p,γ)^{36}Ca reaction. The solid and dot-dashed curves represent the components calculated from the present results and the parameters predicted by Herndl *et al*.[14], respectively.

where A is the reduced mass in atomic mass units, T_9 is the stellar temperature in GK, and E_r is the resonance energy. The resonance strength $\omega\gamma$ is defined as

$$\omega\gamma = \frac{2J+1}{(2J_1+1)(2J_2+1)}\frac{\Gamma_p\Gamma_\gamma}{\Gamma_{\text{tot}}}$$

where J_1, J_2, and J are the spins of the ground states of the incident particles, and target nuclei, and the resonance state of the compound nuclei, respectively. Figure 2 shows the temperature dependence of the reaction rate via the 2_1^+ resonance state. The solid and dot-dashed curves represent the calculated reaction rates based on the present results and theoretical predictions by Herndl *et al*.[14], respectively. The present reaction rate is larger than that predicted by Herndl *et al*. at T < 3 GK, suggesting that the ^{35}K(p,γ)^{36}Ca reaction plays a more important role in explosive hydrogen burning than Herndl *et al*. anticipated. For the ^{26}Si(p,γ)^{27}P reaction, four resonance peaks at 0.315, 0.805, 1.37, and 2.23 MeV, respectively corresponding to the excited states at 1.18, 1.67, 2.23, and 3.1 MeV in ^{27}P, and a direct capture component were observed in the p-^{26}Si relative energy spectrum in a Coulomb dissociation study [4]. Compared with the excited states in the mirror nucleus ^{27}Mg, the spin parities of the states observed at 1.18, 1.67, and 2.23MeV were tentatively assigned to $3/2^+$, $5/2^+$, and $5/2^+$, respectively; since the ground state in ^{27}P has a spin parity of $1/2^+$, these states can be populated by absorption of $M1/E2$, $E2$, and $E2$

virtual photons, respectively. Since the *E*2 virtual photon flux is three orders of magnitude greater than the *M*1 flux at this incident energy, Coulomb dissociation will be sensitive only to the *E*2 component, which is expected to be 20 times smaller than the *M*1 component for the (p,γ) cross section for the first excited state. By fitting experimental data with the detector responses calculated by Monte Carlo simulations, the Coulomb dissociation cross sections for the 1.18, 1.67, and 2.23 MeV states were respectively deduced to be 17.5 (32), 29.8 (53), and 12.6 (31) mb, resulting in $\omega\gamma(E2)$ being 6.5 (13)$\times 10^{-11}$, 6.0 (11)$\times 10^{-10}$, and 1.10 (27) $\times 10^{-9}$ MeV, respectively. The *M*1 component of $\omega\gamma$ of the 1.18-MeV state is evaluated by the shell model to be $1.8^{+1.9}_{-1.1} \times 10^{-9}$ MeV, which leads the total $\omega\gamma$ being $1.9^{+1.9}_{-1.1} \times 10^{-9}$ MeV. The reaction rates of the ^{26}Si$(p,\gamma)^{27}$P reaction at $T = 0.1 - 2$ GK are obtained using the present results. They are slightly lower than previous estimates by Caggiano *et al*. [15] and Guo *et al*. [16]; this is mainly due to the smaller $\omega\gamma$ value of the first excited state in ^{27}P.

3. Proton elastic scattering of ^{26}Si

An alternative study of the ^{26}Si$(p,\gamma)^{27}$P reaction was performed using the CNS RI beam separator (CRIB), which is owned and operated by the University of Tokyo and located on the RIKEN campus. A radioactive ^{26}Si beam was produced by the ^{3}He(^{24}Mg,^{26}Si) reactions at 7.5 MeV/A and separated by CRIB. Since the ^{26}Si beam has a much smaller energy spread than RIPS or Big RIPS, it can be used to perform higher-resolution measurements of proton elastic scattering. Two parallel-plate avalanche counters (PPACs) were used to measure the position of the incident beam. The incident ^{26}Si beam bombarded a thick hydrogen gas target at 330 Torr, which was housed in a 300-mm-radius semi-cylindrical container. The beam particles continuously lose their energy mainly due to hydrogen atoms ionizing and stopped in the gas target. Elastically scattered protons penetrate the target and are detected by a Δ*E*-*E* telescope placed 400 mm downstream of the entrance of the target at $\theta_{\mathrm{lab}} = 0°$. The telescope consisted of a 75-μm-thick double-sided position-sensitive silicon detector (PSD) and two 1.5-mm-thick silicon detectors (SSDs), which both have an area of 50×50 mm^2. The recoil protons passed through the PSD and were stopped in the first SSD. The second SSD was used as a veto counter to eliminate high-energy protons generated upstream of the gas target. The

center-of-mass energy of the ^{26}Si + *p* system is calculated using the measured proton energy and scattering angle event by event. Three obvious peaks were observed at 2.12(3), 2.48(3), and 2.65(3) MeV in the center-of-mass energy spectrum; they correspond to the excited states at 2.98(3), 3.34(3), and 3.50(3) MeV in ^{27}P, respectively. Three additional peaks were found by the *R*-matrix analysis at 2.02(3), 2.54(3), and 2.74(3) MeV; they correspond to the excited states at 2.88(3), 2.40(3), and 3.60(3) MeV, respectively. The spin parities of the 2.98 and 3.50 MeV states were assigned to $1/2^+$ and $5/2^+$, respectively. The $\omega\gamma$ and reaction rate via the 2.98, 3.34, and 3.50 MeV states were estimated with the assistance of shell model calculations [5]. These resonance states were not observed in the Coulomb dissociation study mentioned above. Thus, proton elastic scattering and Coulomb dissociation studies provide complementary information to each other.

4. Direct measurement of the ^{18}Ne(α,*p*) reaction

To study (α,*p*) reactions relevant to the rp process by the direct method, a helium active target using a multiple sampling and tracking proportional chamber with a gas electron multiplier (GEM -MSTPC) was developed. Three dimensional trajectories and energy loss in helium gas was measured using many readout pads with a "backgammon" geometry with a pitch of 4 mm. The ^{18}Ne(α.*p*)^{21}Na reaction was studied using the helium active target. A ^{18}Ne beam was produced by the ^{3}He(^{16}O,^{18}Ne) reaction and separated by CRIB. Two PPACs were used to measure the position of the incident beam. The helium active target was irradiated by the beam. The beam and reaction products were measured by the active target and silicon detectors surrounding the active target.

The detection efficiency of heavy charged particles was about 98% and the deposited energy resolution was 8% in σ for each pad. The reaction position could be determined with resolution in full width of 4 mm. The position resolutions in the horizontal and vertical directions were respectively 2 and 0.1 mm in σ, resulting in a scattering angle resolution of better than 5° in σ.

References

1. S. Wanajo, *Astrophys. J.* **647**, 1323 (2006).
2. M. Arnould and S. Goriely, *Phys. Rep.* **384**, 1 (2003).
3. M. Wiescher *et al*., *J. Phys. G: Nucl. Part. Phys*. **25,** R133 (1999).
4. Y. Togano *et al*., *Phys. Rev*. **C84**, 035808 (2011).
5. H.S. Jung *et al*., *Phys. Rev.* **C85**, 045802 (2012).
6. P. Doornenbal *et al*., *Phys. Lett.* **B647**, 237-242 (2007).
7. N. Iwasa *et al*., Phys. *Rev. Lett.* **83**, 2910 (1999); F. Schümann *et al*., *Phys. Rev*. **C73**, 015806 (2006); T. Kikuchi et al., *Eur. Phys. J.* **A3**, 213 (1998); N. Iwasa *et al*., *J. Phys. Soc. Japan* **65**, 1256 (1996); T. Motobayashi et al., *Phys. Rev. Lett.* **73**, 2680 (1994).
8. T. Motobayashi et al., *Phys. Lett.* **B264**,259 (1991).
9. A. Bürger *et al*., *Eur. Phys. J. Special Topics* **150**, 89 (2007).
10. Detector description and simulation tool by the CERN, Geneva, Switzerland.
11. J. Raynal, coupled channel code ECIS97, unpublished.
12. T. Suomijärvi et al., *Nucl. Phys*. **A509**, 369 (1990).
13. A. M. Bernstein et al., *Phys. Lett.* **B103**, 255 (1981).
14. H. Hendln et al., *Phys. Rev.* **C52**, 1078 (1995).
15. J. A. Caggiano *et al*., *Phys. Rev.* **C64**, 025802 (2001).
16. B. Guo *et al*., *Phys. Rev.* **C73**, 048801 (2006).